East Asian Journal of Multidisciplinary Research (EAJMR)
Vol. 5, No. 11, 2026: 4439 - 4456

A Literature-Grounded Framework for Thermomechanical Modelling of Orthogonal Cutting in Long SiC-Fibre-Reinforced Ti-6Al-4V Composites

DuVan Nguyen
Faculty of Mechanical Engineering, Thu Duc College of Technology, VietNam
Corresponding Author: DuVan Nguyen vandunguyen679@gmail.com

A R T I C L E I N F O

Keywords: Sic-Fibre-Reinforced Ti-6Al-4V, Orthogonal Cutting, Finite-Element Modelling, Thermomechanical Coupling, Interfacial Damage

Received : 14, September
Revised : 15, October
Accepted: 17, November

©2026 Nguyen : This is an open-access article distributed under the terms of the Creative Commons Atribusi 4.0 Internasional.

A B S T R A C T

This study presents a literature-grounded thermomechanical finite-element framework for investigating orthogonal cutting of long SiC-fibre-reinforced Ti-6Al-4V composites under cryogenic (−180 °C), ambient (24 °C), and elevated-temperature (400 °C) conditions. The framework integrates titanium-matrix plasticity, brittle SiC-fibre fracture, fibre–matrix interfacial damage, tool–workpiece contact, and thermal effects. Particular attention is given to the transferability of Johnson–Cook parameters, constitutive-model limitations at cryogenic temperatures, and cohesive-zone calibration. Numerical verification, experimental validation, mesh sensitivity, and parameter uncertainty are incorporated into the proposed workflow. As solver outputs and new experimental measurements are not yet available, quantitative predictions are not claimed. The framework establishes a reproducible basis for future simulation and validated assessment of cutting forces, fracture, and subsurface damage.

DOI prefix: https://doi.org/10.55927/eajmr.v5i11.26
ISSN-E: 2828 – 1519 (Online)
https://eajmrformosa.my.id/index.php/eajmr

INTRODUCTION

Continuous ceramic-fibre-reinforced metal-matrix composites (MMCs) combine the high specific strength and stiffness of ceramic fibres with the toughness and load-bearing capacity of metallic matrices, making them attractive for aerospace and other demanding applications (Hayat et al. 2019; Doorbar and Kyle-Henney 2018). However, machining these heterogeneous materials is challenging because material removal involves titanium-matrix plastic deformation, brittle SiC-fibre fracture, and fibre–matrix interfacial damage. Their interactions can cause irregular fracture, matrix smearing, fibre pull-out, and subsurface damage, complicating surface-integrity prediction and control (Zan et al. 2023; Liao et al. 2019; Han et al. 2021).

Temperature further complicates machining by affecting matrix plasticity, fibre loading, fracture, and interfacial separation. Experiments by (Zan et al. 2023) at approximately −180, 24, and 400 °C demonstrated temperature-dependent material-removal mechanisms, including matrix extrusion between fractured fibres and variations in fibre cracking. These findings highlight the need to model the coupled behaviour of the matrix, fibres, and interfaces rather than treating the composite as homogeneous.

Finite-element modelling provides a means of investigating these mechanisms beyond experimental observations. Previous studies have established the importance of constitutive behaviour, tool–workpiece contact, friction, heat generation, and thermal softening in metal cutting (Meyer and Kleponis 2001; Lesuer 2000; Rodríguez et al. 2020; National Institute of Standards and Technology n.d.; Johnson and Cook 1983; Sima and Özel 2010; Özel and Altan 2000; Shet and Deng 2000; Bäker et al. 2002; Dandekar and Shin 2010; Özel et al. 2021). Composite micromechanics research also emphasizes interfacial bonding, cohesive separation, and damage evolution (Aghdam et al. 2015; Warrier et al. 1999; Camanho and Dávila 2002). Reliable simulations therefore require appropriate material parameters, physically representative fracture and interface laws, and systematic verification and validation (Roache 1998; Oberkampf and Roy 2010; Belytschko et al. 2014).

Cryogenic machining presents a particular modelling challenge because conventional Johnson–Cook-type formulations may not be calibrated for temperatures substantially below their reference temperature. Extrapolation can consequently yield questionable predictions or mathematical difficulties (Meyer and Kleponis 2001; Lesuer 2000; Rodríguez et al. 2020; National Institute of Standards and Technology n.d.; Sima and Özel 2010). Likewise, interfacial strengths and fracture energies cannot be transferred directly between different material systems without justification (Aghdam et al. 2015). These limitations necessitate explicit modelling assumptions, traceable material-property sources, calibration of uncertain parameters, and sensitivity analysis.

This study develops a literature-grounded thermomechanical finite-element framework for investigating temperature-dependent orthogonal cutting of long SiC-fibre-reinforced Ti-6Al-4V. It focuses on the coupled effects of titanium-matrix plasticity, SiC-fibre fracture, interfacial damage, and temperature-dependent material behaviour.

The main contributions of this study are:

a) A thermomechanical finite-element framework for modelling orthogonal cutting of long SiC-fibre-reinforced Ti-6Al-4V composites.
b) A phase-resolved modelling strategy to represent titanium-matrix plasticity, SiC-fibre fracture, and fibre–matrix interfacial damage.
c) A systematic treatment of temperature-dependent material properties and the limitations of conventional constitutive models under cryogenic conditions.
d) A verification and validation strategy incorporating mesh sensitivity, energy balance,parameter uncertainty, and comparison with experimental data.

THEORETICAL REVIEW

Thermophysical response of Ti-6Al-4V

A commonly used nominal density for Ti-6Al-4V is approximately 4,430 kg m^{-3}. Published modelling sources report room-temperature specific heat values around 546–580 J kg^{-1} K^{-1} and thermal conductivity near 7.0–7.3 W m^{-1} K^{-1} (Lesuer 2000; Rodríguez et al. 2020). These values are suitable as documented reference values for an initial model, but a fully coupled analysis should use temperature-dependent data consistent with the alloy condition and the actual temperature interval. NIST provides cryogenic thermophysical data references for Ti-6Al-4V over the low-temperature range (A National Institute of Standards and Technology n.d.).

Table 1. Thermophysical properties of Ti-6Al-4V

Material/input	Adopted reference value	Use in model	Qualification/source
Ti-6Al-4V density	4,430 kg m^{-3}	Mass/inertia and thermal capacity	Literature value (Lesuer 2000; Rodríguez et al. 2020)
Ti-6Al-4V specific heat	546–580 J kg^{-1} K^{-1} near ambient	Thermal capacity	Published values differ; use a temperature curve for coupled analysis (Lesuer 2000; Rodríguez et al. 2020)
Ti-6Al-4V thermal conductivity	7.0–7.3 W m^{-1} K^{-1} near ambient	Heat conduction	Nominal literature values; temperature-dependent function recommended (Lesuer 2000; Rodríguez et al. 2020; National Institute of Standards and Technology n.d.)
Ti-6Al-4V elastic modulus	~110–114 GPa near ambient	Elastic response	Source/model dependent (Lesuer 2000; Rodríguez et al. 2020)
Ti-6Al-4V Poisson ratio	~0.30–0.34	Elastic response	Source/model dependent (Lesuer 2000; Rodríguez et al. 2020)
Melting temperature in JC parameterisations	~1605–1660 °C depending on source/definition	JC thermal normalisation only	Use the exact value paired with the chosen calibration

			(Meyer and Kleponis 2001; Lesuer 2000; Rodríguez et al. 2020)

Constitutive modelling and temperature-range validity

The equation is the Johnson–Cook constitutive model, which describes the equivalent flow stress of a material as a function of plastic strain, strain rate, and temperature:

$$\sigma = (A + B(\epsilon^p)^n)\left[1 + C\ln\left(\frac{\epsilon^p}{\epsilon_0}\right)\right][1 - (T^*)^m] \qquad (1)$$

Where σ is the equivalent flow stress, A is the reference yield stress, B is the strain-hardening coefficient, ϵ^p is the equivalent plastic strain rate, n is the strain-hardening exponent, C is the strain-rate sensitivity coefficient, ϵ_0 is the reference plastic strain rate, T^* is the normalized temperature, m is the thermal softening exponent.

Here

$$T^* = \begin{cases} 0 & ,T <= T_{tr} \\ \frac{T - T_{tr}}{T_m - T_{tr}} & ,T_{tr} < T < T_m \\ 1 & ,T \geq T_m \end{cases} \qquad (2)$$

Where T^* is the dimensionless normalized temperature, ranging from 0 to 1, T is the current material temperature, T_{tr} is the transition or lower reference temperature at which the temperature-dependent contribution begins to be considered, T_m is the melting temperature of the material.

Selection and transferability of Johnson–Cook parameters

Published Ti-6Al-4V parameter sets are not unique. Table 2 lists representative sets reported in the literature (Meyer and Kleponis 2001; Lesuer 2000; Rodríguez et al. 2020). The Meyer–Kleponis set (A = 862.5 MPa, B = 331.2 MPa, n = 0.34, C = 0.012, m = 0.8) is a traceable baseline for conventional high-rate modelling, but it is not a validated temperature-dependent law for the present composite across −180 to 400 °C. At −180 °C, T is below a typical reference temperature of 20–25 °C, so T* becomes negative. For a non-integer m such as 0.8, T* is not real-valued under ordinary real arithmetic. Setting T* to zero or clipping it silently would change the constitutive model and must not be done without justification.

Table 2. Representative Johnson–Cook parameter sets reported for Ti-6Al-4V

Published set	A (MPa)	B (MPa)	n	C	m
Meyer–Kleponis (Meyer and Kleponis 2001)	862.5	331.2	0.34	0.012	0.8
Lee–Lin set 1 (Lesuer 2000)	782.7	498.4	0.28	0.028	1.0
Lee–Lin set 2 (Lesuer 2000)	724.7	683.1	0.47	0.035	1.0
Li–He (Rodríguez et al. 2020)	968	380	0.421	0.0197	0.577
Lesuer/Kay (Lesuer 2000)	1098	1092	0.93	0.014	1.1

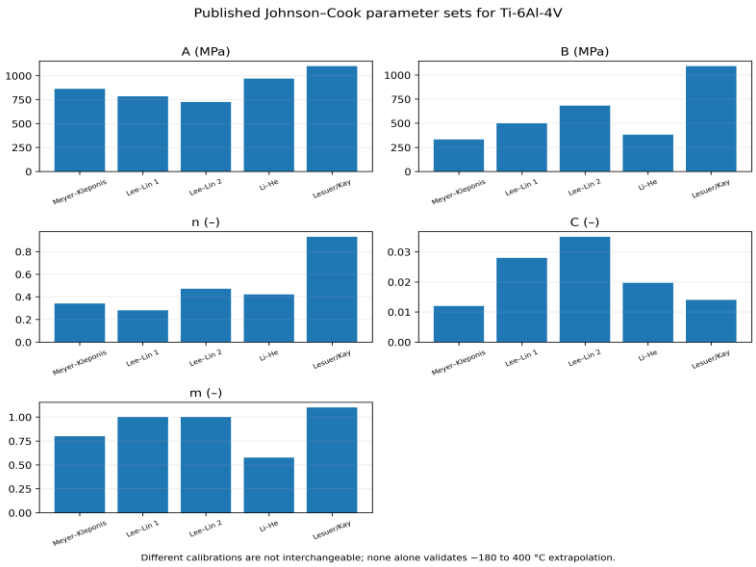


Figure 1. Variability among published Johnson–Cook parameter sets for Ti-6Al-4V.

Implications for the present modelling framework

For quantitative analysis across -180 to 400 °C, the preferred approach is to establish a calibrated flow-stress relationship,

$$\bar{\sigma} = \bar{\sigma}\left(\bar{\varepsilon^p}, \dot{\bar{\varepsilon}^p}, T\right) \quad (3)$$

Using experimental data that cover the relevant temperature, plastic-strain, and strain-rate domains. A modified Johnson–Cook formulation or a physically based constitutive model may also be considered, provided that its functional form is supported by appropriate data and its extrapolation limits are explicitly documented. Finally, the thermal treatment must be consistent with the numerical implementation. If the model prescribes an initial or nominal temperature without solving the fully coupled thermal field, that temperature should not be interpreted as the evolving local temperature of the chip or cutting zone. Conversely, if thermomechanical coupling is implemented, the temperature-dependent constitutive response must be evaluated using the local evolving temperature, with the selected formulation remaining mathematically well-defined throughout the simulated range. These distinctions are essential for ensuring that the predicted cutting forces and damage mechanisms are physically interpretable rather than artefacts of parameter extrapolation or numerical implementation.

Stress invariants and plastic-work measures

For a von Mises matrix model, the equivalent stress is obtained from the deviatoric stress tensor s as

$$\bar{\sigma} = \sqrt{\left(3/2(s):(s)\right)} \quad (4)$$

while the equivalent plastic strain rate is

$$\dot{\bar{\varepsilon^p}} = \sqrt{\left(2/3(\varepsilon)^p : (\dot{\varepsilon})^p\right)} \quad (5)$$

These invariants provide scalar measures for a rate-dependent flow law. They are appropriate for a ductile isotropic matrix but should not be applied indiscriminately to brittle SiC fibres, whose failure is more naturally linked to tensile stress, flaw statistics or fracture mechanics.

$$\dot{W}^p = \sigma : \dot{\varepsilon}^p \quad (6)$$

$$Q^p = \chi \dot{W}^p \quad (7)$$

The coefficient χ is the fraction of plastic work converted into heat. Its value should be taken from a defensible source or treated as uncertain. Under a prescribed-temperature model, this heat-generation term does not update the imposed temperature; under a coupled model, it enters the thermal balance and can influence the local flow stress.

Temperature interpolation and extrapolation control

If tabulated material data are used, interpolate only within the temperature and strain-rate range covered by the source measurements. Piecewise-linear interpolation is transparent and reproducible, but it does not justify extrapolation beyond the end points. Any extrapolation should be separately identified, bounded, and subjected to sensitivity analysis. The cryogenic case is particularly important because a conventional normalized-temperature expression can produce a negative temperature ratio when the reference temperature is above the target temperature.

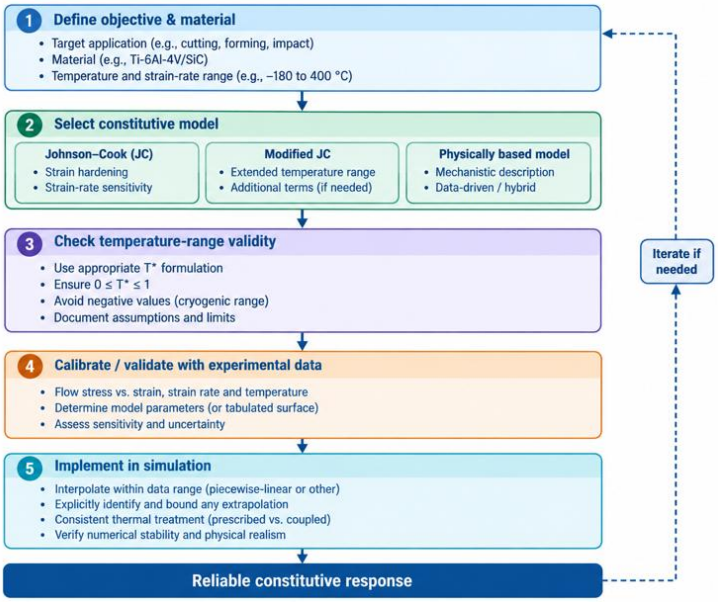


Figure 2. Constitutive selection workflow.

Fibre properties and interface behaviour

The fibre grade and architecture are critical. Literature on SCS-6/Ti-6Al-4V systems reports a fibre fracture stress of about 4.67 GPa in a particular micromechanical model and an interface bond strength of about 140 MPa in a separate experimental/model-based study (Aghdam et al. 2015; Warrier et al. 1999). These are not universal properties of all SiC fibres and must not be transferred automatically to the fibre used by Zan et al. The cited interface bond

strength is also not a Mode-I or Mode-II fracture energy; it cannot be substituted directly for G_Ic or G_IIc in a cohesive-zone law.

Table 3. Fibre/interface data and applicability limits

Input	Traceable literature datum	How used	Critical limitation
SiC fibre tensile fracture stress	4.67 GPa for SCS-6 in a cited SiC/Ti-6Al-4V model (Aghdam et al. 2015)	Candidate comparison only	Grade- and architecture-dependent.
SiC fibre elastic response	Use grade-specific datasheet or measured fibre data	Elastic-brittle constitutive response	Grade-specific; modulus must be verified.
SCS-6/Ti-6Al-4V interface bond strength	140 MPa (Warrier et al. 1999)	Possible normal-strength prior for sensitivity bounds	System-specific; not fracture energy.
Interface G_Ic and G_IIc	No transferable value adopted here	Must measure/calibrate for exact interface	Must be measured or calibrated.
Fibre coating/core dimensions	Measured micrograph / manufacturer grade data	Explicit phase geometry where relevant	Must match the tested composite.

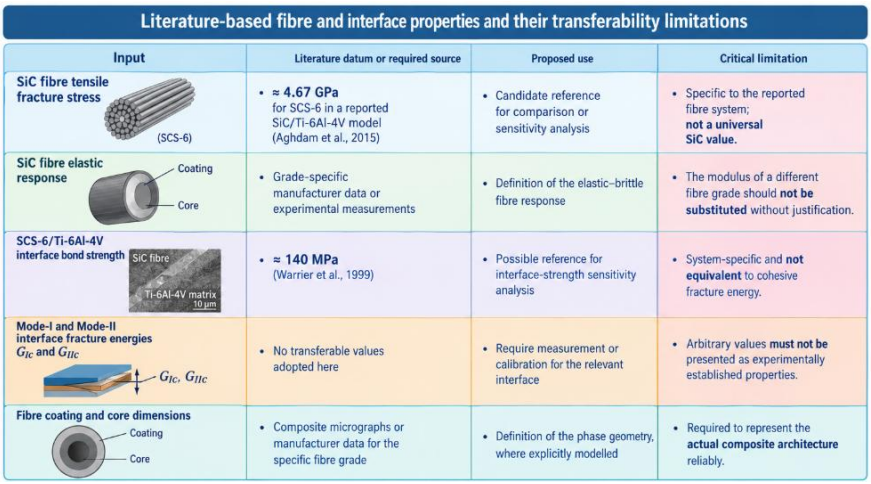


Figure 3. Literature-grounded values and transferability limits. Where the tested fibre grade is unknown, the analogue data are not final model inputs.

Thermomechanical balance equations

For a transient continuum, the momentum balance is

$$\rho \ddot{u} = \nabla \cdot \sigma + b \qquad (8)$$

where b is body force per unit volume (N m^{-3}). If b is instead defined as acceleration (m s^{-2}), the correct form is $\rho \ddot{u} = \nabla \cdot \sigma + \rho b$. The thermal energy balance for a coupled model can be expressed as

$$\rho_{cp} \dot{T} = \nabla \cdot (k \nabla T) + \beta \sigma : \dot{\varepsilon}^{p} + q_{fric} + q_{ext} \qquad (9)$$

where β is the fraction of plastic work converted to heat, q_{fric} is frictional heat generation, and q_{ext} represents other heat sources or sinks. The heat partition between tool and workpiece must be specified. If the simulation is isothermal or

uses a prescribed workpiece temperature, the thermal equation is not solved and this simplification must be declared.

Matrix plasticity and damage

The Ti-6Al-4V matrix may be modelled with a calibrated viscoplastic constitutive law. Ductile damage should be included only if the chosen damage parameters have a traceable calibration and the deletion/regularisation strategy is specified. A generic damage law calibrated for a different Ti-6Al-4V state can alter chip separation and force levels, so the damage model should not be treated as a harmless numerical setting.

Brittle-fibre fracture

The SiC fibre should be represented as an elastic-brittle phase unless grade-specific evidence supports a more complex constitutive response. A maximum principal tensile stress or fracture-mechanics criterion may be used, but local peak stress is mesh-sensitive. The failure criterion should be regularised by a characteristic length or fracture-energy formulation, and fibre strength variability should be represented where statistically relevant. The critical threshold must correspond to the actual fibre grade and coating architecture.

Cohesive interface separation

A cohesive-zone model can represent progressive interface separation using a traction–separation relation. The normal and shear peak tractions, initial stiffness, mixed-mode interaction rule and fracture energies must be independently calibrated or inferred from matching interface tests. The published ~140 MPa bond-strength estimate for SCS-6/Ti-6Al-4V (Warrier et al. 1999) may inform a prior only if the current interface is demonstrably comparable; it is not sufficient to define a complete cohesive law.

Tool–workpiece contact and friction

Use a finite-sliding contact formulation with a documented friction law. A constant Coulomb coefficient is a simplification because tool–chip friction can depend on pressure, temperature, sliding speed and local sticking. The coefficient should be identified from cutting-force data or a relevant independent experiment. Since the present manuscript has no measured force trace available for calibration, no specific friction coefficient is represented as experimentally validated.

METHODOLOGY

Model assumptions and evidence hierarchy

A defensible numerical model separates directly reported experimental conditions from implementation choices and parameters that remain unknown. The primary reference study reports the temperature cases and the figure caption identifies a cutting speed of 50 m/min and depth of cut of 0.1 mm. These source-reported values can define a reference case. Fibre dimensions, exact interface parameters, tool edge radius, friction coefficient and the full constitutive

parameterization must be taken from the complete experimental paper or calibrated independently; they should not be inferred from schematic figures.

Table 4. Evidence hierarchy for model inputs

Evidence class	Definition	How it should be reported	Permitted use
A — exact-source datum	Directly reported for the same material and test	Citation, condition, unit and measured range	Baseline input, subject to implementation checks
B — close analogue	Reported for a related grade or architecture	Explain mismatch and transfer assumption	Sensitivity range; not unquestioned truth
C — calibrated parameter	Estimated against identified independent data	Calibration target, objective function and range	Use only within calibrated domain
D — provisional assumption	Chosen because direct evidence is unavailable	Label explicitly and provide a range	Exploratory sensitivity only

Reference cutting configuration and published conditions

The primary experimental reference is (Zan et al. 2020). Their published figure caption for machined-surface observations specifies a cutting speed of 50 m/min and a depth of cut of 0.1 mm; the paper compares nominal thermal conditions of approximately −180, 24 and 400 °C. These conditions are retained as the reference cases. Other geometric details, including the precise cutting-edge profile, specimen architecture, fibre pitch and fibre coating, must be transcribed from the full experimental methods and microscopy rather than inferred from a schematic.

Table 5. Conceptual phase-resolved cutting geometry

Input	Reference value	Evidence	Status
Cutting speed, v_c	50 m/min (0.833 m/s)	Published surface-analysis figure caption in	Source-reported
Depth of cut	0.1 mm	Published surface-analysis figure caption in	Source-reported
Nominal thermal cases	−180, 24, 400 °C	Experimental	Source-reported
Cutting orientation	Perpendicular to fibre axis	Experimental configuration	Source-reported
Tool rake / clearance / edge radius	Do not assume until extracted from full methods	Strongly affects force and contact stress	Must verify from source
Fibre diameter, pitch, coating and core	Use measured micrograph/grade-specific geometry	Controls phase alternation and stress concentration	Must verify from source

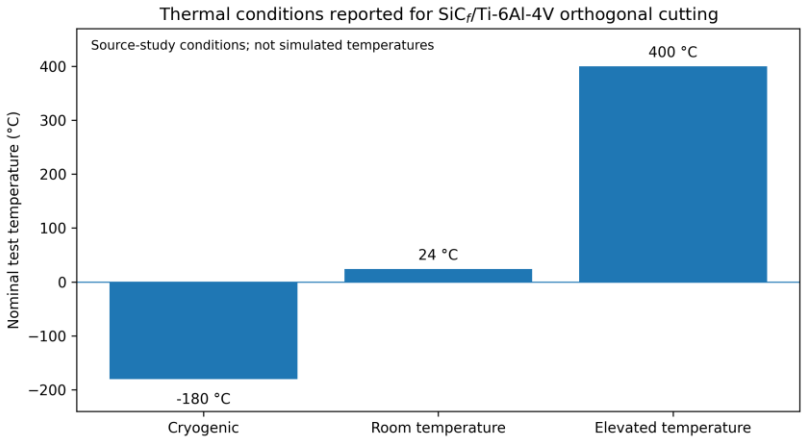


Figure 4. Nominal temperature cases reported by Zan et al. (2023). These are imposed experimental conditions, not computed cutting-zone temperatures.

Computational geometry and dimensionality

A three-dimensional model is preferred to capture fibre bending, finite fibre length, out-of-plane cracking and tool-edge geometry. A 2D plane-strain model is suitable for preliminary screening only, with its limitations clearly stated. Geometry should reflect the actual fibre grade and cross-sectional micrographs, including the core and coating where present; a solid SiC circle is inadequate for coated core–shell fibres.

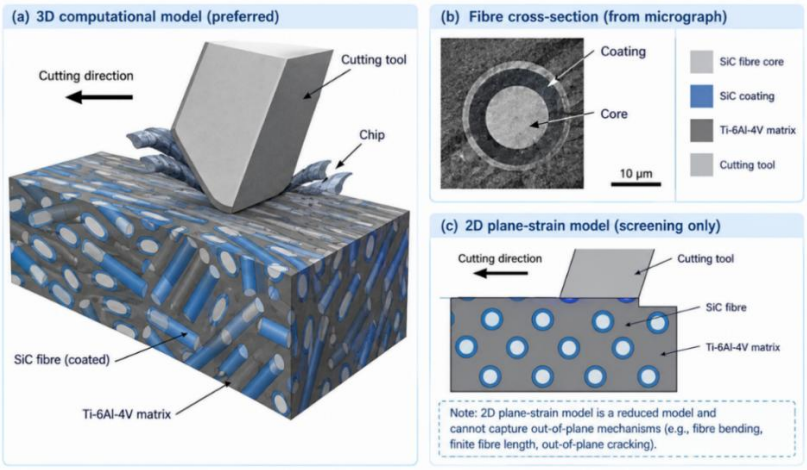


Figure 5. Conceptual phase-resolved cutting geometry.

Thermal and mechanical boundary conditions

The nominal temperatures (−180, 24, and 400 °C) follow the experimental conditions of Zan et al. (2023). Initial temperatures, convection or cryogenic heat transfer, contact conductance, and heat partition must be specified; the cutting zone should not be assumed to remain at the nominal temperature. The cutting speed is 0.833 m s^{-1}, with a depth of cut of 0.1 mm. The workpiece dimensions must minimise artificial boundary effects. If the simulated cutting length is shorter than the reported 10 mm, it should be justified as a local steady-state segment rather than a full experimental reproduction.

Kinematic and thermal definitions

For the published nominal cutting speed Vc = 50 m/min, the SI conversion is Vc = 50/60 = 0.833 m s^{-1}. The depth of cut is 0.1 mm (1.0×10^{-4} m). These values establish the reference kinematics; the actual model domain, tool geometry and fibre layout must still match the experiment. For a fully coupled analysis, thermal contact and frictional heat partition must be specified. For a prescribed-temperature study, report that the selected temperatures are controlled case conditions rather than predictions of transient cutting-zone temperature.

$$V_c = 50/60 = 0.833 \text{ m s}^{-1}, \qquad a_p = 0.1 \text{ mm} = 1.0 \times 10^{-4} \text{ m}$$

Contact, friction and heat partition

For Coulomb friction, the tangential traction magnitude is bounded by the product of the friction coefficient and compressive pressure. A regularized friction law may be needed to avoid numerical discontinuities near zero sliding speed. In coupled thermal analyses, frictional power per unit contact area can be estimated from the product of tangential traction and relative sliding speed; the generated heat is partitioned between tool and workpiece according to a stated thermal model.

$$|\tau_t| \le \mu\, p, \qquad \dot{q}_{fric} = \eta_f\, |\tau_t \cdot v_{slip}| \qquad (10)$$

Here η_f denotes the fraction of frictional power entering the workpiece if $\dot{q}_{fric}$ is defined as workpiece heat flux. The complementary fraction enters the tool or is otherwise accounted for. The notation and units must be consistent with whether heat generation is defined per unit area or per unit volume.

Mesh design and numerical procedure

Mesh refinement should be concentrated near the cutting edge, fibre boundaries and expected fracture path. A minimum of three systematically refined meshes is required. Report element type, element counts, local element size, stable time increment, mass scaling (if used), deletion settings and the force averaging window. Convergence must be evaluated using mean force and integrated damage/fracture measures; raw maximum stress at a singular interface point is not an appropriate convergence metric.

Cohesive damage evolution and energy regularization

For a bilinear cohesive law, damage initiation is defined by a peak-traction criterion and damage evolution by the reduction of traction with increasing effective separation. A generic scalar damage variable D ranges from 0 (intact interface) to 1 (fully separated), with traction represented schematically as t = (1 − D) K δ after damage initiation. The exact mixed-mode initiation and evolution equations depend on the selected cohesive formulation and must be specified in the solver input and manuscript.

$$G_c = \int_0^{\delta f} t(\delta) d\delta\,, 0 \le D \le 1 \qquad (11)$$

The area under the traction–separation curve is the fracture energy per unit area. If the same physical fracture energy is not preserved as the mesh changes,

the apparent debond length and dissipated energy may become mesh dependent. Report the cohesive element size, peak tractions, fracture energies, mixed-mode rule and any viscosity or stabilization parameter.

Table 6. Minimum cohesive-zone specification

Parameter	Symbol	Unit	Required disclosure
Initial normal/shear stiffness	Kn, Ks	Pa m^{-1}	Source or numerical penalty rationale
Peak normal/shear traction	tn0, ts0	Pa	Material-specific calibration or sensitivity bounds
Mode-I fracture energy	GIc	J m^{-2}	Interface evidence and temperature dependence
Mode-II fracture energy	GIIc	J m^{-2}	Interface evidence and mixed-mode rule
Damage evolution law	D(δ)	—	Exact law and regularization method
Cohesive element length	le	m	Mesh-refinement study

Numerical verification

Verification asks whether the discretised equations are solved consistently. At minimum, perform (i) mesh refinement, (ii) time-step/stability sensitivity, (iii) domain-size sensitivity, (iv) energy balance checks, (v) contact-penetration checks, and (vi) regularisation sensitivity for fracture. Report force convergence only after excluding start-up transients and defining the averaging interval in advance.

Validation strategy

Validation requires comparison with independent experimental measurements under matching conditions. For cutting force, use the same force component, width normalisation, cutting speed, depth of cut, temperature and averaging definition. For damage, compare observable quantities such as fibre-crack locations, damaged-layer depth or crack density from microscopy/XCT, with uncertainty and image-resolution limits stated. The published mechanisms in (Zan et al. 2023) provide qualitative targets, but a visual resemblance to published micrographs is not a quantitative validation metric.

Parameter uncertainty and sensitivity

The principal uncertain inputs include the temperature-dependent flow stress of the titanium matrix, the strength distribution of the SiC fibres, the cohesive parameters of the fibre–matrix interface, the tool–workpiece friction coefficient, and the actual fibre geometry. Each input should be documented by source, calibration range, and uncertainty where available. Parameters lacking direct evidence should be treated as uncertain assumptions rather than validated material constants. Quantitative uncertainty intervals for model outputs should be reported only after simulations have been performed over defensible input ranges.

Reproducible finite-element workflow

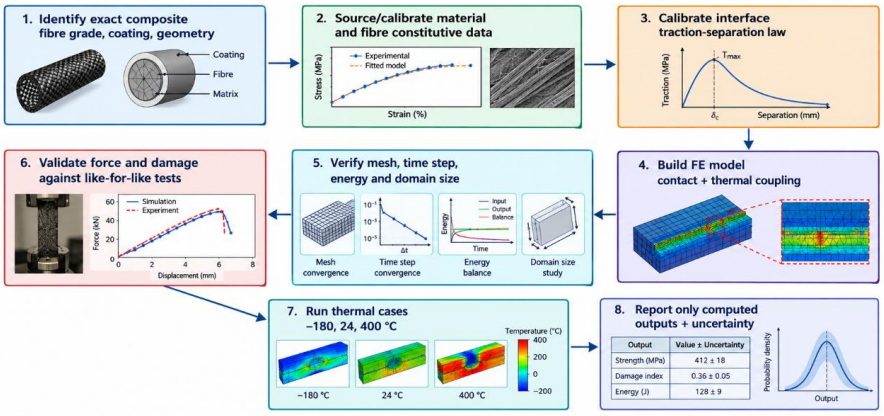


Figure 6. Recommended sequence for an auditable model.

RESEARCH RESULTS

Post-processing definitions and reporting rules

The same post-processing window and thresholds must be used for all temperatures. The steady-cutting interval should be identified from the tool-engagement history and documented; it must not be selected independently to favour a desired result. Cutting-force averages should be reported with the corresponding signal window, sampling interval and any filtering. Damage metrics should be defined against a common final-surface datum and observation window so that differences are not artifacts of inconsistent post-processing.

$$\bar{F}_x = \left(\frac{1}{\Delta t}\right)\int_{t_1}^{t_2} F_x(t)dt \qquad (12)$$

$$U_c = \frac{\int_{t_1}^{t_2} F_x(t)V_c dt}{V_{(removed)}} \qquad (13)$$

Here $\Delta t = t_2 - t_1$ and Vremoved is the volume removed over the same interval. If specific cutting energy is reported, the definition must be dimensionally consistent and the removed volume must be calculated from the actual geometry and cutting distance. For a 2D model, force is often reported per unit width; the normalization must be stated explicitly.

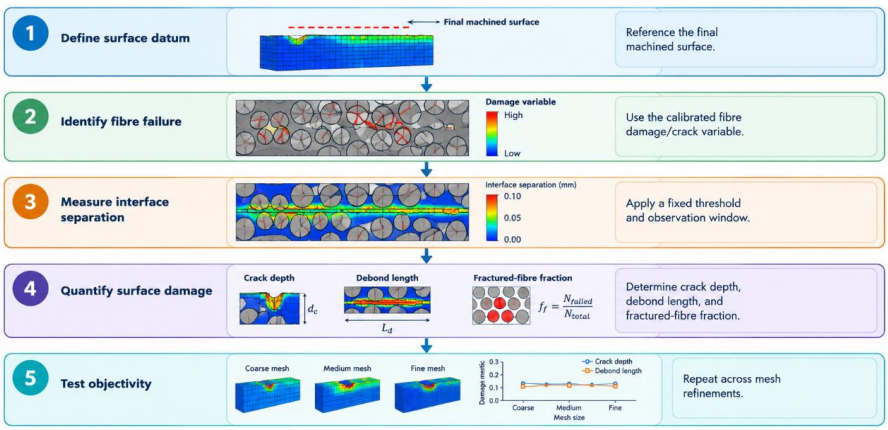


Figure 7. Proposed damage-metric extraction workflow

Table 7. Definitions for comparable simulation outputs

Metric		
Mean cutting force	Time average of Fx over a defined steady interval	State interval and width normalization
Peak cutting force	Maximum Fx within the same stated interval	Separate physical peaks from start-up transients
Specific cutting energy	Cutting work divided by removed volume	State volume calculation and force convention
Maximum damage depth	Farthest damage point below final machined surface	Use common datum and mesh-sensitivity test
Debond length	Sum of interface segments above a declared damage threshold	Report threshold and observation window
Fractured-fibre fraction	Number of failed fibres divided by fibres in window	Define failure criterion and counting rule

Temperature-Dependent Mechanisms Reported in the Literature

(Zan et al. 2023)report that the cutting mechanism in SiC_f/Ti-6Al-4V is governed by the ordered alternation between the ductile matrix and brittle fibres. They observed matrix extrusion between fractured fibres and differences in the machined surface under cryogenic, room-temperature and elevated-temperature conditions. Their results support the hypothesis that matrix stiffness/strength affects the support provided to adjacent fibres and therefore the local fibre-fracture process. These are source-study observations, not results calculated by the present framework.

Testable Hypotheses for the Three Temperature Cases

The cryogenic, ambient and elevated-temperature cases should be interpreted as a controlled comparison. At −180 °C, the question is whether the calibrated matrix response increases resistance to deformation and how that affects load transfer to fibres. At 24 °C, the case establishes a reference for the same geometry and numerical settings. At 400 °C, the question is whether matrix softening changes force while altered interface or fracture behaviour changes damage. The sign and magnitude of these effects are outputs to be determined, not assumptions to be embedded in the conclusions.

Table 8. Hypotheses and evidence needed for temperature comparison

Case	Hypothesis to test	Primary output	Necessary caution
−180 °C	Cryogenic matrix response changes force and stress transfer	Force history; crack depth; debond length	Requires a cryogenic-valid constitutive law
24 °C	Reference force–damage response	All defined metrics	Use as baseline only after verification
400 °C	Matrix softening may lower force but alter damage	Force; energy; damage metrics	Interface/fibre temperature effects may be unknown
Across cases	Trend remains stable under parameter uncertainty	Normalized response changes	Use common mesh, definitions and uncertainty ranges

Status of quantitative simulation outputs

No finite-element solver outputs or new experimental measurements are available for the present manuscript. Accordingly, cutting forces, fibre stresses, interface-damage measures, subsurface damage depths, and mesh-convergence values are not reported as computed results. The present analysis is therefore limited to literature-supported mechanisms, model-development requirements, and testable hypotheses for the three temperature cases. Quantitative conclusions will require model execution, numerical verification, and validation against independent experimental data under comparable cutting conditions.

Table 9. Summary of simulation outputs, reporting criteria, and current computational status

Output to report after simulation	Definition / reporting rule	Current status
Mean cutting force	Mean over pre-defined steady interval; report N and N/mm if width-normalised	Not computed
Force fluctuation	RMS or coefficient of variation over same interval	Not computed
Fibre tensile stress	Prefer percentile or volume-averaged metric; state sampling region	Not computed
Interface damage	Area fraction or cohesive dissipation; define metric precisely	Not computed
Subsurface damage depth	Geometric depth from final surface to deepest validated damage feature	Not computed
Mesh convergence	Change between at least three meshes for force and damage metrics	Not computed
Validation error	Relative error vs. like-for-like measured reference	Not computable without outputs/data

Table 9 summarises the quantities required for subsequent numerical reporting and identifies their current computational status. Mean cutting force, force fluctuation, fibre tensile stress, interface damage, subsurface damage depth, mesh convergence, and validation error remain unreported because the required solver outputs and, where applicable, experimental reference data are not available. The table is a reporting template and should not be interpreted as evidence of completed numerical analysis.

DISCUSSION

Conditions for quantitative interpretation

Figure 1 shows substantial variation among published Johnson–Cook parameter sets, highlighting the risk of inaccurate cutting-force predictions without validation. Uncertainty is particularly high under cryogenic conditions, where conventional thermal-softening formulations may be unreliable. Moreover, SCS-6 interface properties (Aghdam et al. 2020) may not represent the unspecified SiC fibre grade considered here.

Quantitative trends should therefore be reported only after obtaining reference measurements, identifying the fibre architecture, and calibrating the

matrix and interface models. Table 4 provides the reporting framework without assuming uncomputed results.

Parametric analysis and design implications

After baseline validation, sensitivity analysis should examine the matrix flow-stress curve, fibre strength, interface strength and fracture energy, friction, and fibre geometry over physically justified ranges. Mesh refinement and alternative regularisation lengths should also be assessed.

Temperature affects not only matrix behaviour but also load transfer between the tool, matrix, and fibres. Consequently, force and damage trends must be established through validated simulations rather than assumed from temperature alone.

Quantitative sensitivity and decision criteria

A first-order local sensitivity can be estimated by perturbing one input parameter while holding all others fixed. For smooth responses, the local sensitivity of output Q to parameter p can be estimated using a central difference:

$$Sp \approx (p_0/Q_0) \cdot [Q(p_0+\Delta p) - Q(p_0-\Delta p)]/(2\Delta p) \qquad (14)$$

A process recommendation should be constrained by both productivity and damage. A candidate temperature can be considered only if the force or energy remains below the relevant equipment limit and damage metrics remain within application-specific tolerances. Those tolerances must be supplied by design requirements or experiments; they cannot be derived from an unvalidated simulation alone.

Feasible condition: $F_x \le F_{lim}$; $d_{crack} \le d_{lim}$ and $L_{debond} \le L_{lim}$

Table 10. Proposed decision matrix after validation

Decision objective	Metric	Constraint / comparison	Use
Machine/tool loading	Mean and peak cutting force	Below machine/tool allowable limit	Reject overloaded conditions
Energy demand	Specific cutting energy	Compare within uncertainty bounds	Rank energy efficiency
Surface integrity	Crack depth and debond length	Below component-specific tolerance	Reject damage-prone conditions
Robustness	Sensitivity/uncertainty interval	Trend persists across plausible inputs	Prefer robust process window

CONCLUSIONS AND RECOMMENDATIONS

This study establishes a literature-grounded finite-element framework for investigating thermomechanical orthogonal cutting of long SiC-fibre-reinforced Ti-6Al-4V composites. The framework distinguishes titanium-matrix plasticity, brittle-fibre fracture, and fibre–matrix interfacial separation, while addressing the limitations of transferring constitutive and interface parameters across material systems and temperature ranges. The proposed methodology defines the requirements for model construction, numerical verification, experimental validation, and consistent extraction of cutting-force and damage metrics. However, quantitative predictions for the −180, 24, and 400 °C cases remain

unavailable until the model is implemented, calibrated, and validated against compatible experimental measurements. Before using the framework for process selection, the exact fibre architecture and interface properties should be established, the temperature-dependent constitutive response should be calibrated, and mesh sensitivity and predictive accuracy should be demonstrated. Only then can the effects of temperature on cutting force, fibre fracture, and subsurface damage be evaluated quantitatively.

FURTHER STUDY

Future work will focus on validating the proposed finite-element framework against experimental data, calibrating material and interface parameters, and assessing mesh sensitivity and model uncertainty. Subsequent parametric studies will investigate how cutting conditions and fibre–matrix interactions affect cutting forces, fibre fracture, and subsurface damage, supporting reliable machining recommendations.

ACKNOWLEDGMENT

The author gratefully acknowledges the Faculty Mechanical Engineering, Thu Duc College of Technology, Vietnam, for providing the academic environment and institutional support for this study.

REFERENCES

S. Zan, Z. Liao, J.A. Robles-Linares, G. Garcia Luna, D. Axinte, et al., Machining of long ceramic fibre reinforced metal matrix composites – How could temperature influence the cutting mechanisms? International Journal of Machine Tools and Manufacture 185 (2023) 103994. https://doi.org/10.1016/j.ijmachtools.2023.103994.

M.D. Hayat, H. Singh, Z. He, P. Cao, Titanium metal matrix composites: an overview. Composites Part A: Applied Science and Manufacturing 121 (2019) 418–438. https://doi.org/10.1016/j.compositesa.2019.04.005.

P.J. Doorbar, S. Kyle-Henney, Development of continuously-reinforced metal matrix composites for aerospace applications. In: Comprehensive Composite Materials II, Elsevier (2018), pp. 439–463. https://doi.org/10.1016/B978-0-12-803581-8.09983-5.

Z. Liao, A. Abdelhafeez, H. Li, Y. Yang, O.G. Diaz, D. Axinte, State-of-the-art of surface integrity in machining of metal matrix composites. International Journal of Machine Tools and Manufacture 143 (2019) 63–91. https://doi.org/10.1016/j.ijmachtools.2019.05.006.

H.W. Meyer, D.S. Kleponis, Modeling the high strain rate behavior of titanium undergoing ballistic impact and penetration. International Journal of Impact Engineering 26 (2001) 509–521.

J.M. Rodríguez, S. Larsson, J.M. Carbonell, P. Jonsén, Dislocation density based flow stress model applied to the PFEM simulation of orthogonal cutting processes of Ti-6Al-4V. Materials 13(8) (2020) 1979. https://doi.org/10.3390/ma13081979. This article tabulates multiple published Johnson–Cook parameter sets, including the Li–He set used for

comparison here.
National Institute of Standards and Technology (NIST), Cryogenic Materials Properties: Ti-6Al-4V, thermal conductivity and linear thermal expansion data/reference list. https://trc.nist.gov/cryogenics/materials/Ti6Al4V/Ti6Al4V_rev.htm.
Simulation of interface damage in metal matrix composites under off-axis loading using cohesive zone model. Computational Materials Science 108 (2015) 42–47. https://doi.org/10.1016/j.commatsci.2015.05.030.
G.R. Johnson, W.H. Cook, A constitutive model and data for metals subjected to large strains, high strain rates and high temperatures. Proceedings of the 7th International Symposium on Ballistics (1983) 541–547.
M. Sima, T. Özel, Modified material constitutive models for serrated chip formation simulations and experimental validation in machining of titanium alloy Ti-6Al-4V. International Journal of Machine Tools and Manufacture 50 (2010) 943–960. https://doi.org/10.1016/j.ijmachtools.2010.08.004.
T. Özel, T. Altan, Determination of workpiece flow stress and friction at the chip–tool contact for high-speed cutting. International Journal of Machine Tools and Manufacture 40 (2000) 133–152. https://doi.org/10.1016/S0890-6955(99)00051-6.
[14] M. Shet, X. Deng, Finite element analysis of the orthogonal metal cutting process. Journal of Materials Processing Technology 105 (2000) 95–109. https://doi.org/10.1016/S0924-0136(00)00578-6.
[15] M. Bäker, J. Rösler, C. Siemers, A finite element model of high speed metal cutting with adiabatic shearing. Computers & Structures 80 (2002) 495–513. https://doi.org/10.1016/S0045-7949(02)00023-8.
P.P. Camanho, C.G. Dávila, Mixed-mode decohesion finite elements for the simulation of delamination in composite materials. NASA/TM-2002-211737 (2002).
W.L. Oberkampf, C.J. Roy, Verification and Validation in Scientific Computing. Cambridge University Press (2010).
T. Belytschko, W.K. Liu, B. Moran, K. Elkhodary, Nonlinear Finite Elements for Continua and Structures, 2nd ed. Wiley (2014).
X. Han, D. Xu, D. Axinte, Z. Liao, H.N. Li, On understanding the specific cutting mechanisms governing the workpiece surface integrity in metal matrix composites machining. Journal of Materials Processing Technology 288 (2021) 116875. https://doi.org/10.1016/j.jmatprotec.2020.116875.
C.R. Dandekar, Y.C. Shin, Laser-assisted machining of a fiber reinforced metal matrix composite. Journal of Manufacturing Science and Engineering 132 (2010). https://doi.org/10.1115/1.4002548.
T. Özel, et al., Numerical Analysis of Serrated Chip Formation Mechanism with Johnson-Cook Parameters in Micro-Cutting of Ti6Al4V. Metals 11 (2021) 102. https://doi.org/10.3390/met11010102.